

Ammonia Removal in Activated Carbons Prepared from Olive Oil Industry Waste

Victor Ferrer,¹*,^{a,b} Mauricio Flores,^a Héctor Grandón,^a Néstor Escalona^{a,c,d,e} and Cristina Segura^a

^aUnidad de Desarrollo Tecnológico (UDT), Universidad de Concepción,
Av. Cordillera 3624, Parque Industrial Coronel, CP 4191996, Coronel, Biobío, Chile

^bCentro Nacional de Excelencia para la Industria de la Madera (CENAMAD),
Pontificia Universidad Católica de Chile, Av. Vicuña Mackenna 4860, CP 7820436, Santiago, Chile

^cDepartamento de Ingeniería Química y Bioprocesos, Facultad de Ingeniería,
Pontificia Universidad Católica de Chile, Avenida Vicuña Mackenna 4860, CP 6904411, Santiago, Chile

^dANID-Millennium Science Initiative Program-Millennium Nuclei on Catalytic Process Towards
Sustainable Chemistry (CSC), CP 6904411, Chile

^eCentro de Investigación en Nanotecnología y Materiales CIEN-UC,
Pontificia Universidad Católica de Chile, Avenida Vicuña Mackenna 4860, CP 6904411, Santiago, Chile

Activated carbons (ACs) from olive stone were prepared using CO₂, steam, KOH, and H₃PO₄ as activating agents. The resultant activated carbons were characterized by proximate and ultimate analysis, N₂ adsorption (Brunauer-Emmett-Teller (BET) method), iodine number, Boehm titration, temperature-programmed desorption (TPD), and Fourier transform infrared spectroscopy (FTIR). Ammonia (NH₃) was used as a test molecule to be adsorbed. The BET surface areas of the ACs obtained ranged from 1000 to 1986 m² g⁻¹. Type I isotherms were obtained for all the samples, although steam and H₃PO₄ ACs showed a significant mesopore contribution. KOH activation resulted in carbon with a high microporosity (98%) and high iodine adsorption (1030 mg g⁻¹). KOH AC prepared with a KOH/pyrolyzed char weight ratio of 2 and at 900 °C showed the highest NH₃ adsorption (252 mg g⁻¹), favored by the high microporosity and adequate acidity. Chemical activation (KOH and H₃PO₄) promotes higher NH₃ adsorption than the physical ACs prepared (CO₂ and steam). Langmuir and Freundlich adsorption equilibrium models were used to correlate the NH₃ adsorption isotherms, obtaining the best fit for the Freundlich equation. The results indicated that olive stone-based activated carbon could be used for commercial AC to remove NH₃ from gaseous streams.

Keywords: olive stones, activated carbon, physical and chemical activation, adsorption isotherms, ammonia removal

Introduction

Activated carbon (AC) is a well-known material employed to separate and remove unwanted substances present in industrial effluents. Because of its affordable price, high porosity, internal surface area, and excellent adsorptive capabilities, AC is the most extensively used adsorbent.¹ This material is commonly used in the chemical and food industries, as well as other process industries (drinking water treatment, pharmaceuticals, etc.).²

Physical and chemical activations are employed to prepare activated carbons (ACs). In the physical method, the raw material is carbonized between 400 and 800 °C, followed by gasification at higher temperatures in an oxidizing gas flow (steam, CO₂, air, or a combination).^{3,4} Hence, the physical activation is a two-step process but can also be done in a one-step process.⁵ Carbonization and activation are carried out simultaneously in chemical activation, using a chemical substance (e.g., H₂SO₄, H₃PO₄, ZnCl₂, KOH, NaOH) and then subjected to a heat treatment (500-800 °C) in a one-step process.^{6,7} The surface area, porosity, and adsorption properties of AC are determined by the type of the raw material, as well as

*e-mail: v.ferrer@udt.cl

Editor handled this article: Jaísa Fernandes Soares

the method and process parameters used for carbonization and activation.^{8,9}

Anthracite, peat, lignite, bituminous coal, and lignocellulosic materials such as coconut shells and wood are among the most popular carbon-containing feedstocks employed as a precursor to producing AC.¹⁰ In the last decades, an increasing number of investigations related to the production of low-cost AC from agricultural wastes such as sugarcane bagasse,¹⁰ pistachio-nut shells,¹¹ corn-cob,³ date stones,¹² neem husk,¹³ almond shell,⁹ fir bark,¹⁴ jackfruit,¹⁵ cherry stones,¹⁶ coffee grounds,¹⁷ rice husk,¹⁸ peach stones,¹⁹ palm kernel shell,²⁰ and olive stones,²¹⁻²³ have been reported. These ACs have displayed good performance and could replace expensive coal-based carbons in various industrial applications to remove different pollutants (e.g., dyes, metal ions, organic pollutants, pharmaceuticals and personal care products). The AC prepared from an abundant waste source would include economic gains and environmental benefits.

In this sense, the olive agribusiness in Chile has about 25,000 hectares of olive trees, with a production of 18,500 tons of oil in 2019 destined for the national and international market, ranking Chile in tenth place among the olive oil-exporting countries in the world.²⁴ The oil extraction process generates about 70,000 tons of solid waste, an organic residue with high humidity that is used directly on soils as fertilizer, compost, or fuel in the same process.²⁵⁻²⁷ However, a large part of this waste is not used and is accumulated, generating environmental problems associated with foul odors.²⁸

The pyrolysis process of agricultural by-products has been considered a technology to solve the disposal problem associated with this waste.^{9,23,29-31} Using this process, it is possible to generate add-value products such as liquids and gases with fuel characteristics, and the char can be used as a precursor of the AC.⁹ The proposed technological solution aims to strengthen the olive industry in Chile through the integral recovery of its residues through the development of ACs, taking advantage of the intrinsic characteristics of the olive stone.

For this reason, the goal of this study is to evaluate the use of the olive stone to obtain ACs by physical (CO₂ and steam) and chemical activation (KOH and H₃PO₄), testing them for NH₃ adsorption and establishing which method can promote the best AC for the proposed application. Although olive stone as a raw material for obtaining AC has been widely studied,^{1,4,8,22,32-39} few investigations have focused on simultaneously evaluating the four activations carried out in this work. Concerning NH₃, this gas is one of the most commonly released compounds in the chemical industry, and its presence can be smelt in the air even at low

concentrations (< 50 ppm), causing eye, throat, and nose irritation.^{40,41} The use of AC is a promising approach to removing this gas, considering its simplicity and economic operation.⁴² Besides, it has been reported that the acidic surface functionalities of AC favor NH₃ adsorption and the direct interaction between the gas molecules and the carbon surface.⁴³ Therefore, the production of AC from the waste of olive oil production can become one of the solutions for the effective elimination of residues and contribute to the sustainability and competitiveness of small and medium-sized industries in this sector.

Experimental

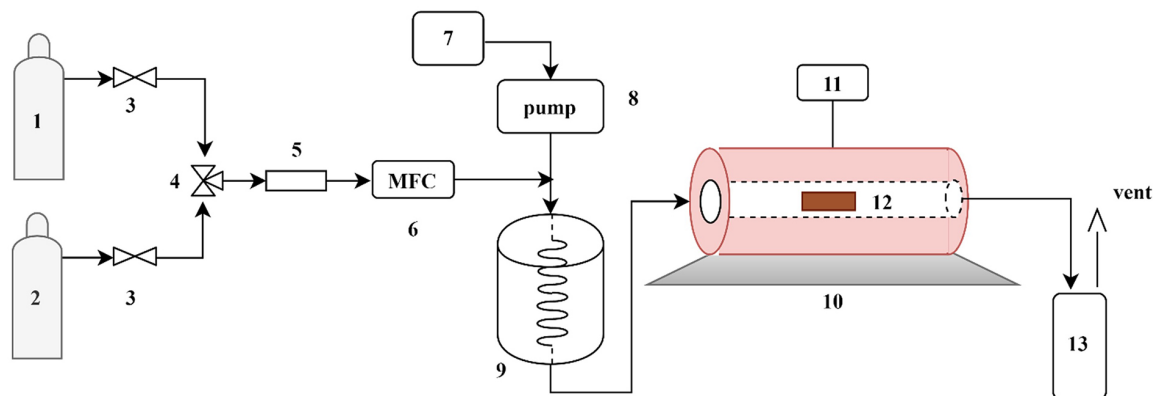
Materials

Olive stones were supplied by a local olive oil manufacturer (Terramater, Curicó Valley-Region of Maule, Chile). These materials were processed without previous treatment, crushed and sieved until particle sizes between 0.6 and 1 mm were obtained. For comparison purposes, the C Gran and GAC 1240 Norit (Cabot Corporation, Massachusetts, USA) commercial ACs were included in the analysis (see Supplementary Information section).

Preparation of ACs

ACs were prepared using physical and chemical methods. Physical activation was done employing CO₂ (Linde, 99.5%, Santiago, Chile) and steam, and for chemical activation, KOH (Merck, 85% purity, Darmstadt, Germany) and H₃PO₄ (Merck, 85% purity, Darmstadt, Germany) reagents were used. After reviewing some references, the conditions to pyrolyze and activate the material were considered.^{5,7,10,11,22,35,44-50}

The experimental apparatus used in this research for the preparation of AC is shown in Figure 1. First, olive stones' pyrolysis (carbonization) was carried out in a MELLER PS205 horizontal furnace (New Hampshire, USA) at 400 and 600 °C for 1 h with a heating rate of 5 °C min⁻¹ and a N₂ (Linde, 99.995%, Santiago, Chile) flow rate of 150 mL min⁻¹. About 40 g of raw material in the alumina ceramic crucible was placed into the furnace. After pyrolysis, the furnace was cooled to room temperature (ca. 20 °C) with a N₂ flow. The designations OS-400 and OS-600 refer to olive stones that have been pyrolyzed at 400 and 600 °C, respectively. The pyrolytic char produced at 600 °C was used for ACs prepared in a two-step procedure.



1. N₂ 2. CO₂ 3. On-off valve 4. 3-way valve 5. Filter 6. Mass flow controller
7. Water 8. Peristaltic pump 9. Steam generator 10. Oven 11. Temperature controller 12. Sample 13. Condenser

Figure 1. Schematic diagram of the pyrolysis/activation experimental system.

CO₂ activation

The pyrolytic char (4 g) was activated at 850 °C (heating rate of 10 °C min⁻¹) with a CO₂ (Linde, 99.999%, Santiago, Chile) flow rate of 100 mL min⁻¹, keeping the temperature for 1 h. In this case, the sample was obtained in a two-step activation process. For comparison, the raw material (40 g) was directly activated without being previously pyrolyzed, following the one-step activation procedure. The prepared samples were designated as AC-CO₂ 1 and AC-CO₂ 2, and the numbers 1 or 2 correspond to the activation in one or two-step, respectively.

Steam activation

The previously pyrolyzed olive stone (6.5 g) and the raw material (20 g) were activated in the system indicated above at 900 °C for 1 h, keeping a steam/N₂ (Linde, 99.99%, Santiago, Chile) ratio equal to 4. Next, the samples were heated to the temperature required for activation in N₂ flow (200 mL min⁻¹) with a heating rate of 10 °C min⁻¹. The steam was introduced into the furnace after the temperature was reached. The steam was generated by injecting 0.6 mL min⁻¹ of liquid water into an evaporator by a peristaltic pump (equivalent to 800 mL min⁻¹ of steam determined at 20 °C and 101.32 kPa). After activation, the samples (AC-H₂O 1 and AC-H₂O 2) were cooled to room temperature under N₂ flow.

KOH activation

The pyrolyzed char was impregnated with a concentrated KOH solution in the required proportion to obtain two slurries with a KOH/pyrolyzed char weight ratio of 1 or 2. The slurries were heated at 70 °C

until incipient dryness. The samples were then dried overnight at 105 °C. After that, the activation was done for 1 h in a N₂ flow of 300 mL min⁻¹ and a heating rate of 5 °C min⁻¹. Activation was carried out at 800 and 900 °C. Once activated, the first washing was carried out with 0.1 mol L⁻¹ HCl (Merck, 37%, Darmstadt, Germany) solution and later with distilled water until obtaining a pH > 5. The samples were identified as AC-KOH 1-800, AC-KOH 1-900, AC-KOH 2-800, and AC-KOH 2-900, whose numbers 1 or 2 are related to KOH/pyrolyzed weight ratio, and the number 800 or 900 corresponds to the activation temperature. The one-step method was not evaluated for this activation method because the previous test resulted in a low yield (< 11%). It is desirable to produce an AC that has a relatively high yield.

H₃PO₄ activation

The olive stone and pyrolytic char were mixed with an adequate quantity of a H₃PO₄ solution to obtain a H₃PO₄/sample weight ratio of 1.75. This mixture was stirred at 70 °C until dry and kept on a stove at 105 °C overnight. It was then activated for 1 h at 600 °C (heating rate: 3 °C min⁻¹; N₂ flow: 300 mL min⁻¹). Finally, the carbon was washed with hot water until pH > 5 and dried at 105 °C to be later stored. The ACs were named AC-H₃PO₄ 1 and AC-H₃PO₄ 2, where the numbers 1 and 2 indicate if the sample was activated in one or two-step.

On completion, the resultant ACs by different methods were weighed to determine their yield. Here, the global yield (Y_G) of char or AC is calculated by dividing the sample weight after activation (W_f) by the weight of the raw material (W_i) using the following equation:

$$Y_G (\%) = (W_f/W_i) \times 100 \quad (1)$$

Using the pyrolyzed sample as the starting point, an equation was used to figure out the yield (Y_p) of the ACs prepared with the two-step method:

$$Y_p(\%) = (W_p/W_i) \times 100 \quad (2)$$

where W_p is the weight of pyrolyzed sample.

Characterization of ACs

Proximate analysis was done following the ASTM D1506⁵¹ and ISO 562⁵² standards to determine the content of ash and volatiles, respectively, while the moisture was determined after drying the sample at 105 °C overnight. Ultimate analysis was performed in a Leco CHNS 628 (Michigan, USA) elemental analyzer equipment.

Textural properties were obtained from the N_2 adsorption-desorption isotherm at -196 °C with a Micromeritics 3-Flex instrument (Georgia, USA). The samples (30-50 mg) were pretreated at 300 °C in a vacuum condition for 4 h in the Micromeritics SmartVacPrep equipment (Georgia, USA). The Brunauer-Emmett-Teller (BET) method was used to determine the specific surface area, employing the adsorption branch of the isotherms in the range of $0.02 \leq P/P_0 \leq 0.25$.^{53,54} The amount of N_2 adsorbed at $P/P_0 = 0.99$ corresponds to the total pore volume, including the micro and mesopores.⁵³ All pores in the adsorbent are assumed to be filled with condensed gas at this point. The Dubinin-Radushkevich equation was used to calculate the volume of micropores.⁵⁵ The volume of mesopores was obtained as the difference between the total volume and the volume of micropores.

The sodium thiosulfate volumetric method was used to determine the iodine number expressed as the milligrams of iodine adsorbed by 1 g of carbon.⁵⁶ Briefly, the powder AC and a 0.05 mol L⁻¹ iodine solution (Supelco, Reag. Ph Eur, Darmstadt, Germany) are mixed, shaken, and then the filtrate is submitted to titration against a standardized 0.1 mol L⁻¹ Na₂S₂O₃ solution (Merck, Darmstadt, Germany).

The surface oxygenated functional groups were determined following the Boehm method.⁵⁷ The four 0.1 g of samples were mixed with 20 mL of 0.05 mol L⁻¹ of NaOH (Winkler, 98.6%, Santiago, Chile), Na₂CO₃ (Sigma-Aldrich, 99.5%, Massachusetts, USA), NaHCO₃ (Winkler, > 99%, Santiago, Chile), and HCl (Merck, 37%, Darmstadt, Germany) solutions, respectively. The vials were sealed and stirred for 24 h in a thermal bath at 25 °C. The suspensions are filtered and titrated by 0.05 mol L⁻¹ HCl or 0.05 mol L⁻¹ NaOH solutions. The numbers of the acidic sites were calculated considering that NaOH neutralizes carboxylic, lactonic and phenolic groups;

Na₂CO₃ neutralizes carboxylic and lactonic, and NaHCO₃ neutralizes only carboxylic groups. The amount of HCl that reacted with the AC was used to calculate the number of basic sites.

The chemical nature of the surface was analyzed by temperature-programmed desorption followed by mass spectrometry (TPD-MS), using the same apparatus described in the textural properties test (Micromeritics 3-Flex instrument) coupled with a mass spectrometer (Cirrus 2, MKS Spectra Product, Andover-Massachusetts, USA). The sample (0.05 g) was pre-conditioned in He flow at 45 °C for 1 h before the desorption runs. After that, the sample was heated up to 1000 °C at a heating rate of 10 °C min⁻¹ in He flow (100 mL min⁻¹). A quadrupole mass spectrometer was used to detect the amount of CO₂ and CO desorbed as a function of temperature. Calibration was done with calcium oxalate monohydrate for quantification.

The pH of the point of zero charge (pH_{pzc}) is the pH at which the surface's net charge is zero.⁵⁸ 0.1 g of samples were placed in Erlenmeyer flasks with 50 mL of NaCl (Riedel-de Haën, 99.8%, Germany) 0.01 mol L⁻¹ solution. The initial pH (pH_i) was adjusted between 2-12 values using NaOH or HCL solutions of 0.1 mol L⁻¹ and a PL-700PC Gondo instrument pH meter (Taipei, Taiwan). Then, the suspension was shaken for 48 h, and the pH of the filtrate was measured (pH_f). The pH_{pzc} was obtained from the plot of pH_f vs. pH_i and corresponded to the value where pH_f is equal to pH_i .

The surface functional groups of carbons were identified using the Fourier transform infrared spectroscopy (FTIR) technique. A Bruker Alpha FT-IR spectrometer was used to record the samples' FTIR spectra between 4000 and 400 cm⁻¹ (Billerica, Massachusetts, USA). First, pellets were prepared by mixing carbon and KBr (1:400 carbon/KBr weight ratio) in an agate mortar. Then, in a hand press, the resulting mixture was compressed.

NH₃ adsorption

Adsorption equilibrium data of NH₃ were carried out in the same equipment employed for the textural properties test (Micromeritics 3-Flex instrument). Before measurement, 50 mg of sample was treated in He flow at 300 °C for 4 h and then exposed to the increasing pressure of anhydrous NH₃ (Indura, 99.5%, Santiago, Chile) up to 90 kPa at room temperature. The adsorption equilibrium amount was calculated at the terminal pressure from the final adsorption amount.

The experimental data were fitted to the Langmuir and Freundlich isotherms.⁵⁹ The Langmuir isotherm is expressed as:

$$q_c = (a_m \times b \times P)/(1 + b \times P) \quad (3)$$

where q_c is the adsorbed NH_3 amount *per* unit mass of solid ($\text{cm}^3 \text{g}^{-1}$), a_m is the maximum adsorption capacity of the solid (mg g^{-1}), b is the Langmuir adsorption constant related to the adsorption energy (kPa^{-1}), and P is the NH_3 pressure (kPa).

The Freundlich isotherm is given by:

$$q_c = K_F \times P^{1/n} \quad (4)$$

where K_F ($\text{cm}^3 \text{g}^{-1} \text{kPa}^{-1/n}$) and n are the constants, relate to the relative capacity adsorption of adsorbent and the adsorption intensity, respectively.^{59,60}

Nonlinear regression is used to determine all the parameters from the experimental points. The fitness degree was estimated by the coefficient of determination (R^2), and the average relative error (ARE) was calculated by the equation:⁶¹

$$\text{ARE} (\%) = \left(\sum_1^N \frac{q_{\text{exp}} - q_c}{q_{\text{exp}}} / N \right) \times 100 \quad (5)$$

where q_{exp} is the experimentally adsorbed amount of NH_3 , q_c is the amount of NH_3 calculated using the models, and N is the number of adsorption points.

Results and Discussion

Starting and pyrolyzed material

Table 1 shows the properties of the raw and pyrolyzed olive stone. The olive stone is characterized by the high volatiles content and carbon and low ash values.^{62,63} For comparison purposes, the olive stone was pyrolyzed at two temperatures (400 and 600 °C). This sample's proximate and ultimate analysis results are compared with those reported by the references mentioned above, although the moisture can vary between 5 to 10%.⁶⁴ Sulfurous was not detected in the sample. After pyrolysis of olive stone, the content of volatiles decreased while the carbon increased. It is well known that the increase in temperature promotes the degradation of the constituents of the olive stone (hemicellulose, cellulose

and lignin), and these components can be volatilized, and inorganic material (ash) is concentrated.⁶⁵ As a result of the large quantity of volatiles generated during pyrolysis, yields diminish as the temperature rises from 400 to 600 °C.¹¹ The OS-600 sample was used to produce the AC due to the higher C content compared to OS-400.

Characterization of ACs

The proximate and ultimate analysis results and the yield of the ACs are given in Table 2. The values are similar for all samples and close to the commercial ACs analyzed. The activation increases the carbon content, and the ash tends to concentrate. The %H decreased after the activation treatments, and the nitrogen content remained low, varying between 0.5-1%.³⁴

It is desirable to produce an AC with a relatively high yield, and depending on whether activation was carried out in one- or two-step, this parameter will be affected. When the global yield is considered, the one- and two-step activations report lower yields (20%), except when H_3PO_4 is used as an activating agent for the one-step method (40%). When CO_2 is used as an activating agent, and the sample is activated in one-step (AC- CO_2 1), a yield of 17% was obtained. The global yield remained in the same order (19%) when the activation was carried out in two steps (AC- CO_2 2 sample). The yield (Y_p) significantly increased up to 70% when calculated from the pyrolyzed olive stone as a starting material. It has been reported that the partial gasification of the raw material or char exposed to CO_2 occurs by the following equation:⁸



In this sense, both the effect of a high temperature and CO_2 presence promotes the precursor decomposition and increases the extent of the reaction,⁵ causing a decrease in yield (or increased burn-off). In the case of two-step activation, the yield is higher since a large part of the volatiles have already been released.

In steam activation, water reacts with the carbon of the sample to produce carbon monoxide and hydrogen, according to:⁸

Table 1. Properties of raw and pyrolyzed olive stone

Sample	Proximate analysis / wt. %				Ultimate analysis / wt. %			Y_G / %
	Ash	Moisture	Volatiles	Fixed carbon ^a	C	H	N	
Olive stone	0.66	9.05	86.85	12.49	51.96	6.45	0.25	–
OS-400	1.25	1.16	13.62	85.13	80.08	4.01	0.45	35
OS-600	1.15	2.89	18.64	80.21	90.59	2.52	0.46	27

^aDry basis. Y_G : global yield.

Table 2. Proximate and ultimate analysis and yield of ACs

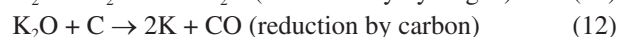
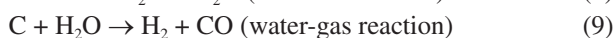
Sample	Proximate / wt. %				Ultimate / wt. %			Y _G / %
	Ash	Moisture	Volatiles	Fixed carbon ^a	C	H	N	
AC-CO ₂ 1	2.12	4.05	9.72	88.16	92.90	0.95	0.86	17
AC-CO ₂ 2	2.02	3.27	12.33	85.65	95.87	1.11	0.76	19 (70)
AC-H ₂ O 1	3.57	1.59	10.90	85.53	92.05	1.09	0.59	11
AC-H ₂ O 2	3.19	1.25	8.14	88.67	94.21	0.90	0.66	10 (37)
AC-KOH 1-800	2.35	1.68	14.47	83.18	92.33	0.59	0.81	20 (76)
AC-KOH 2-800	1.46	4.65	12.50	86.04	93.45	0.58	1.02	17 (63)
AC-KOH 1-900	1.93	0.84	15.78	82.29	89.61	0.60	1.04	17 (64)
AC-KOH 2-900	5.30	1.15	22.44	72.26	86.90	0.68	0.97	17 (62)
AC-H ₃ PO ₄ 1	3.22	1.49	17.43	79.35	87.82	0.98	0.65	40
AC-H ₃ PO ₄ 2	5.12	0.17	11.18	83.70	90.23	2.37	0.49	18 (68)
Norit GAC 1240 ^b	3.95	5.89	9.65	86.40	91.37	0.36	0.88	–
Norit C Gran ^b	2.59	4.77	22.55	74.86	82.73	2.79	0.70	–

^aDry basis; ^bcommercial AC. Values in parenthesis correspond to yield Y_p; Y_G: global yield.



Therefore, the carbon is consumed, and porosity (micro and mesopores) can be generated. The use of steam or CO₂ makes physical activation more advantageous than chemical activation, requiring more expensive and toxic chemicals and consecutive washing processes to eliminate excess reagents. The global yield obtained for steam activation in one- or two-step was low, registering values between 10 and 11%. During this process, weight loss occurs both due to the evolution of volatile material and the elimination of carbon atoms through steam reaction (equation 6). This low yield agrees with previous research,⁶⁶ which indicated that low solid yields (or high burn-off) and high generation of volatiles are associated with steam's capacity to penetrate the solid material, helping the removal and efficient desorption of volatile products. In the case of the AC-H₂O 2 sample, a yield of 37% was obtained, employing the pyrolyzed sample mass as starting material. This result is because the sample activated with steam was previously pyrolyzed, and a large part of the volatiles was removed.

For chemical activation, specifically the KOH activation, it has been established that this method consists of redox reactions, with the carbon oxidation to CO or CO₂.⁴⁹ As shown below, KOH activation involves a sequence of reactions, including dehydration, water gas reaction, and reduction by hydrogen and carbon.⁶⁷ During these reactions, the biomass is broken down, resulting in the generation of micropores and mesopores structures.



The increase in the KOH/precursor ratio and the temperature causes a slight decrease in the global yield, obtaining 20 and 17% of yield for AC-KOH 1-800 and AC-KOH 2-900 samples, respectively. These yields were 76 and 62% for the previously mentioned samples when calculated from the pyrolyzed material mass, and the effect of the KOH/precursor ratio and temperature on the yield was more evident. Metallic potassium is obtained due to KOH reduction or its transformation products (e.g., K₂CO₃).⁵⁰ The solid particle breaks down when potassium is intercalated within the graphitic lamellar structure, making granular carbon preparation difficult. This explains why the carbon obtained from this activation turned into a fine powder, and high temperatures or KOH concentration affected the yield.

In addition, the direct activation of the raw olive stone produces a very light material due to the breakdown of the precursor particles after KOH solution impregnation. The attack of hydroxyl ions causes the fragmentation and dissolution of lignin and hemicellulose.³⁹ It explains the meager yield obtained (< 11%) in the preliminary test using unpyrolyzed olive stone and why it was not used in the AC preparation.

When H₃PO₄ was used as an activating agent, a Y_G of 40 was obtained for the AC-H₃PO₄ 1 sample, while the AC-H₃PO₄ 2 sample registered a Y_G of 18% (68%, considering the pyrolyzed material). This trend is similar to that observed for the evaluated physical activations. As mentioned before, the sample impregnation generates

reactions that promote cellulose fragmentation and other structural components of the olive stone, so the raw material is more affected than the pyrolyzed char. Because the acid separates the cellulose fibers and causes partial depolymerization of hemicellulose and lignin, the particle treated with H_3PO_4 becomes elastic, causing a decrease in mechanical resistance and particle swelling. Similarly, because many tars have been detected on the particle's surface, impregnation promotes carbon conversion.⁴⁵ These tars come from acid-catalyzed cellulose depolymerization, dehydration, and condensation, resulting in aromatic and reactive compounds with some cross-linking.

Figure 2 depicts the nitrogen adsorption-desorption isotherms for the physically and chemically activated samples, while Table 3 reports the textural properties obtained from the adsorption isotherms. All the carbons presented type I isotherms, characteristic of predominant

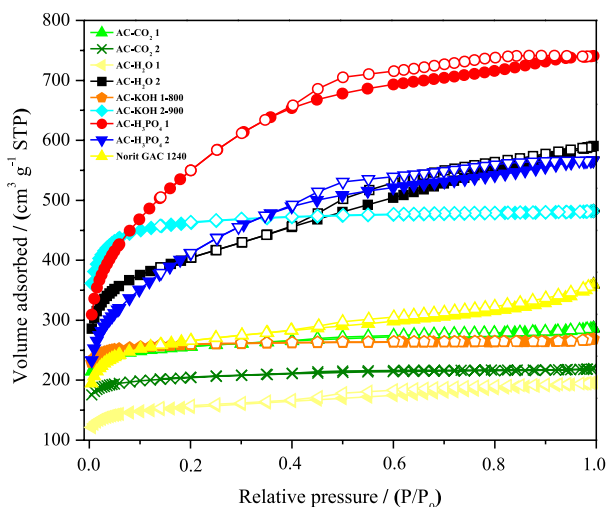


Figure 2. N_2 adsorption-desorption isotherms at $-196\text{ }^\circ\text{C}$ of ACs. Closed symbols: adsorption curve and open symbols: desorption curve.

Table 3. Textural properties of samples prepared by physical and chemical activation

Sample	S_{BET} / ($\text{m}^2\text{ g}^{-1}$)	V_{mi} / ($\text{cm}^3\text{ g}^{-1}$)	V_{me} / ($\text{cm}^3\text{ g}^{-1}$)	V_{tot} / ($\text{cm}^3\text{ g}^{-1}$)	D^a / nm	V_{mi}/V_{tot} / %
Olive stone	5	0	0.006	0.006	4.64	0
OS-600	131	0	0.015	0.015	4.64	0
AC-CO ₂ 1	1011	0.395	0.047	0.442	1.75	89
AC-CO ₂ 2	810	0.314	0.025	0.339	1.67	93
AC-H ₂ O 1	597	0.237	0.066	0.303	2.02	78
AC-H ₂ O 2	1511	0.603	0.309	0.912	2.41	66
AC-KOH 1-800	1052	0.405	0.009	0.415	1.57	98
AC-KOH 2-900	1823	0.731	0.015	0.745	1.63	98
AC-H ₃ PO ₄ 1	1986	0.735	0.411	1.146	2.31	64
AC-H ₃ PO ₄ 2	1491	0.551	0.325	0.876	2.35	63
Norit GAC 1240	1016	0.414	0.142	0.556	2.19	75
Norit C Gran	1328	0.531	0.588	1.119	3.37	47

^a $4 \cdot V_{tot} / S_{BET}$. S_{BET} : BET surface area; V_{mi} : micropore volume; V_{me} : mesopore volume; V_{tot} : total pore volume; D : average pore diameter.

microporous solids. For samples activated with CO_2 and KOH , a percentage of micropores ($\%V_{mi}/V_T$) higher than 90% was obtained, while the carbons obtained by steam and H_3PO_4 activation showed a micro-mesoporous structure.^{8,38,67,68}

For micro-mesoporous carbons, an H4-type hysteresis loop was observed, usually found in solids that consist of aggregates or agglomerates of particles with slit-shaped pores.³ These samples showed percentages of micropores between 60–78%, with an average pore diameter very close to 2 nm, indicative that small mesopores are present. It has been reported that CO_2 activation favors the creation of microporosity while the use of steam increases microporosity at the beginning of the activation, which are then transformed into mesopores, obtaining carbons with a lower percentage micropore than CO_2 -activated samples.^{35,69}

The chemically activated samples showed the highest surface areas, highlighting the AC-KOH 2-900 ($1823\text{ m}^2\text{ g}^{-1}$) and AC- H_3PO_4 1 ($1986\text{ m}^2\text{ g}^{-1}$) samples. For the KOH -activated samples, increasing the KOH /precursor ratio (from 1 to 2) and the activation temperature (from 800 to $900\text{ }^\circ\text{C}$) improves the surface area. This result can be expected because more KOH is intercalated into the material structure, favoring the porosity generation during impregnation and subsequent activation.^{38,70} It has been reported the presence of mesopores when wood carbons were activated with H_3PO_4 , while the carbons obtained by KOH activation reported a microporous structure.⁷¹

The one-step sample activated with CO_2 (AC- CO_2 1) has a surface area of $1011\text{ m}^2\text{ g}^{-1}$, a higher value than the sample activated in a two-step (AC- CO_2 2, $810\text{ m}^2\text{ g}^{-1}$). However, the percentage of micropores did not change (ca. 90%). This same behavior was reported for H_3PO_4 -

activated carbons, where the surface area of AC-H₃PO₄ 1 was higher than AC-H₃PO₄ 2. The opposite trend was observed for the steam-activated sample, whose surface area of the AC-H₂O 1 sample (597 m² g⁻¹) was lower than that activated in a two-step (AC-H₂O 2, 1511 m² g⁻¹). These results indicate the importance of the initial contact surface with the activating agent and the temperature, activation time, activating agent flow, and heating ramp that influence the diffusion and removal of gaseous products from the surface of the coal.^{4,5,34}

It is well known that the non-carbonized substance interacts with the activating agent more intensely than the carbonized material.³⁸ Hence, carbons obtained in one-step activation show higher BET surface area (S_{BET}) than carbons prepared in two-step activation (using OS-600 sample for the steam activation). However, this behavior was not observed for steam-activated samples. It is possible that the one-step activation conditions were very aggressive, consuming the sample and the destruction of pores. This hypothesis is established considering the low global yield obtained for the two activated carbons (AC-H₂O 1 and AC-H₂O 2) and other investigations,^{2,3} indicating that the external burning of carbon particles affects the porosity. For carbons prepared in the two-step activation, the sample carbonized in nitrogen has a more organized structure and less developed porosity than carbonized in steam. This fact is related to a lower reaction rate for the nitrogen-carbonized sample.⁷²

The iodine number allows one to quantify the AC's adsorptive capacity and can be used to determine pores with dimensions ≥ 1.0 nm.⁴⁴ Iodine number of the samples with the highest surface area by each method and commercial carbons is reported in Table 4. Chemical KOH activation generates a carbon with high iodine adsorption capacity, with an iodine number of 1030 mg g⁻¹ for AC-KOH 2-900 sample, even higher than those obtained for commercial carbons. Considering that iodine adsorption is indicative of the adsorption capacity in micropores,⁷³ this result is well-correlated with its textural properties (Table 3) because a high percentage of micropores was reported

(98%). The other carbons showed a lower iodine number than the KOH sample. It may be due to the creation of meso and macropore structures, thus decreasing the adsorptive capacity of iodine.² Similar values of iodine number for carbons based on olive stone have been reported by other researchers.^{29,36,74}

Boehm titration results of selected carbons are shown in Table 4. The chemistry of the surface and the porosity have a significant impact on the performance of ACs. Acidic groups include carbonyl, carboxyl, phenolic hydroxyl, and lactonic groups, whereas basic groups include pyrene, chromene, quinone, and the graphene structure's electrons.⁷⁵ The AC surface's acid/base nature is determined by the groups and delocalized electrons of the graphitic structure.⁷⁶ Depending on the activation method and preparation conditions, functional groups on the carbon surface with a wide range of concentrations are favored.⁷⁴

Acidic surface groups decompose at high temperatures, implying that high activation temperatures favor low acidity.⁷⁷ Because of this, physically activated carbons (like CO₂ and steam) tend to be basic, which is in line with the pH_{pzc} values (7.8 and 8.2, respectively) found in Table 4 and shown in Figure S1 (SI section). Therefore, the surface groups in the AC-CO₂ 1 and AC-H₂O 2 samples are mostly basic. The same trend was registered for the AC-KOH 2-900 sample. In this sense, carbons prepared from hazelnut bagasse and activated with KOH (KOH/precursor mass ratio between 1-3) have predominantly basic surface groups.⁶ The sample activated with KOH registered the highest amount of carboxylic groups, with total values of the basic groups slightly higher than acidic groups. This result promotes a little acidic pH_{pzc} value (6.7).

On the other hand, treatment with H₃PO₄ generates an activated carbon of an acidic nature (pH_{pzc} = 3.2), with fewer carboxylic groups than the sample activated with KOH. However, this sample recorded the highest content of phenolic groups. These results are consistent with those registered in the TPD tests, obtaining a more remarkable CO₂ evolution in the sample activated with KOH. In

Table 4. Iodine adsorption and Boehm titration of selected carbons

Sample	Iodine number / (mg g ⁻¹)	Boehm / (mmol g ⁻¹)					pH _{pzc}
		Carboxylic	Lactonic	Phenolic	Acidic	Basic	
AC-CO ₂ 1	775	1.18	0.20	0.59	1.97	4.00	7.8
AC-H ₂ O 2	683	0.98	0.88	0.29	2.15	5.20	8.2
AC-KOH 2-900	1030	1.77	0.59	1.18	3.53	5.20	6.7
AC-H ₃ PO ₄ 1	718	1.57	0.88	1.67	4.12	3.30	3.2
Norit GAC 1240	959	0.59	0.29	0.69	1.57	2.60	6.9
Norit C Gran	706	1.38	1.08	0.98	3.43	2.80	3.6

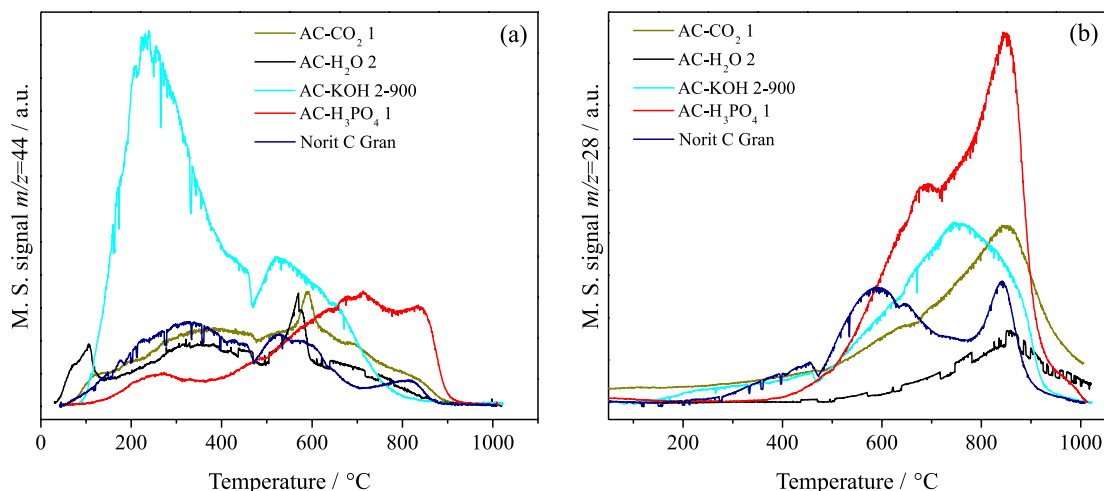


Figure 3. Desorption profiles of ACs obtained by TPD-MS. (a): CO₂ evolution, (b): CO evolution.

contrast, the one activated with H₃PO₄ showed a higher evolution of CO.

For AC-H₃PO₄ 1 sample, a higher proportion of acid groups was generated, a result also obtained by other researchers.^{58,74,78} In general, the acidic content of chemically prepared ACs was higher than those that were physically activated, and similar pH_{pzc} values were reported.^{58,79-81} The commercial activated carbons Norit GAC 1240 and C Gran showed pH_{pzc} measurements related to their neutral and acid nature.⁸²

The total capacity of oxide groups increased using H₃PO₄ as an activating agent. The generation by surface oxidation of acidic functional groups containing oxygen and/or phosphorous and its attachment to the surface while the porosity is being developed has been proposed.⁸³ Even in the case of ACs prepared using H₃PO₄, the carboxylic group is thought to be the only strong acidic group detectable by NaHCO₃.^{69,84,85} The -OH group linked to phosphorus-containing acids adsorbed on the surface has been partly responsible for the surface's strong acidity (i.e., -PO₂H₂).⁸⁶ Based on the investigation mentioned before, it is suggested that the acidic groups detected should be considered as both oxygen-containing and oxygen/phosphorus acidic groups.

The surface chemistry of the ACs was evaluated using temperature-programmed desorption (TPD) experiments coupled to mass. The temperature at which CO and CO₂ are evolved during TPD can characterize the functional groups that contain oxygen. The CO₂ and CO desorption profiles obtained by TPD-MS are shown in Figure 3, while the amounts desorbed are compiled in Table 5. It has been proposed as a general trend that CO₂ evolves at temperatures between 300 and 800 °C and corresponds to the degradation of the surface oxygen groups that are more acidic and less stable. At temperatures near 300 °C, carboxylic groups degrade to CO₂, followed by lactones and

anhydrides (which give both CO and CO₂) at temperatures above 800 °C. CO is produced by the decomposition of the oxygen groups that are the most stable and least acidic, such as anhydride and phenolic groups at 600 °C, and of carbonyls and quinone at temperatures that can reach 900 °C.⁸⁷⁻⁹¹

Table 5. Amounts of CO and CO₂ desorbed measured by TPD-MS

Sample	CO ₂ / (mmol g ⁻¹)	CO / (mmol g ⁻¹)
AC-CO ₂ 1	1.315	2.076
AC-H ₂ O 2	1.091	0.636
AC-KOH 2-900	3.306	3.372
AC-H ₃ PO ₄ 1	1.352	5.170
Norit C Gran	1.132	2.421

AC-KOH 2-900 sample (Figure 3a) showed the highest value for CO₂ evolution (3.306 mmol g⁻¹), which can be explained by the high degree of more acidic surface groups, such as carboxylic groups. The presence of this acidic group was also corroborated by the Boehm and FTIR characterization. As will be discussed later, the existence of this surface oxygen group plays an essential role in NH₃ adsorption. For AC-H₃PO₄ 1 sample, the CO₂ TPD profile shows the majority presence of lactones and/or anhydrides groups. At the same time, the region related to the decomposition of carboxylic groups did not have a significant contribution to the profile. This observation could corroborate the hypothesis raised concerning the overestimation of carboxylic groups in the Boehm treatment.

The CO desorption profiles are shown in Figure 3b. AC-H₃PO₄ 1 sample had the highest CO evolution (5.170 mmol g⁻¹), registering broadband between 350 and 1000 °C with a maximum at 848 °C and a shoulder near

686 °C. The signal at 686 °C is attributed to phenol and hydroquinones, while the maximum at 848 °C is assigned to carbonyl and quinones.⁹²

The difference in the oxygenated surface groups was noticed depending on the chemical agent used for the activation. For KOH activated sample (AC-KOH 2-900), oxygenated surface groups degrade primarily as CO₂ (anhydrides, lactones, carboxylic acid, etc.) during TPD tests, while for H₃PO₄ activated sample (AC-H₃PO₄ 2), those groups decompose as CO (carbonyl, semiquinone, etc.) are the most numerous.³⁸ In this sense, the oxygen-phosphorous bond in the C–O–P system is the weakest in H₃PO₄ activated samples. Therefore, this bond is broken at high temperatures, leaving only an O atom linked to a carbon site and favoring the CO desorption.⁹³

FTIR spectra of the obtained ACs are shown in Figure 4. The assignments of various bands observed are listed in Table 6. The presence of the oxygen functional groups was determined by the FTIR, which agrees with the Boehm results. The samples' spectra were very similar,

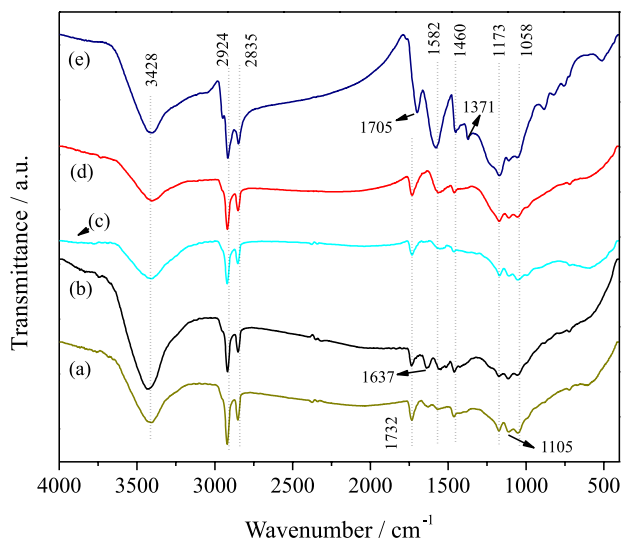


Figure 4. FTIR (KBr) spectra of ACs: (a) AC-CO₂ 1; (b) AC-H₂O 2; (c) AC-KOH 2-900; (d) AC-H₃PO₄ 1; (e) Norit C Gran.

Table 6. Assignments of infrared bands observed in the ACs prepared

Band position / cm ⁻¹	Assignment
3428	OH stretches in hydroxyl, carboxylic and phenolic groups ^{15,94}
2924, 2835	C–H stretching modes in aliphatic ^{15,95}
1732, 1705, 1637	C=O and C–O stretching of carboxylic acid, phenolic ester and conjugated ketonic structures ^{95,96}
1582	C=C stretching in aromatic rings ^{97,98}
1460	C–O stretching vibration from the carboxyl group ^{15,94}
1371	asymmetric bending vibration of the -CH ₃ group ^{15,94}
1173	stretch vibration of C–C, C–O or C–H from the carboxyl groups (–COOH) ⁹⁴
1105, 1058	C–O group in carboxylic and alcoholic groups ^{70,99}
Below 1000	aromatic, out of plane C–H bending with different substitution degrees ⁹⁵

and an intense band at 3428 cm⁻¹ for AC-H₂O 2 sample can be noticed. Considering that this sample was activated using steam and the band can also be assigned to adsorbed water,⁹⁴ the contribution of water on the spectrum is not ruled out.

It has been reported in H₃PO₄ ACs prepared from woody biomass, a broadband between 900–1300 cm⁻¹ with a maximum at 1116–1142 cm⁻¹. This band is related to oxygen and phosphorous compounds in the ACs.⁷⁴ In our results, considering the similarity of the carbons' spectra that were prepared using different methods and the overlap of the absorption bands, an unambiguous assignment is complex, and just the presence of phosphorous compounds can be suggested.

For Norit C Gran commercial AC, the intense band at 1582 cm⁻¹ indicates a more non-polar (hydrophobic) surface than the other prepared carbons.¹⁵

NH₃ adsorption

NH₃ adsorption isotherms of the selected samples at 20 °C are plotted in Figure 5. The maximum amount of NH₃ adsorbed was determined from these isotherms and is reported in Table 7. The volume adsorbed indicates a high adsorption capacity for all the ACs prepared compared to other carbons discussed in the literature and the commercial ones used as references. For example, AC-KOH 2-900 AC reports the higher NH₃ volume adsorbed (332.9 cm³ g⁻¹), corresponding to 252 mg g⁻¹. The high adsorption capacity obtained for the samples could be due to the oxygen functional groups, especially the carboxylic groups.¹⁰⁰ Figure 6 depicts the interaction between the ammonia molecule and the carboxylic groups of ACs.

Boehm titration, FTIR and TPD results have demonstrated the presence of acidic functional groups (phenolic, lactonic and carboxylic) that can explain the high NH₃ adsorption capacity obtained. It has been found that an increase in the number of functional oxygen groups

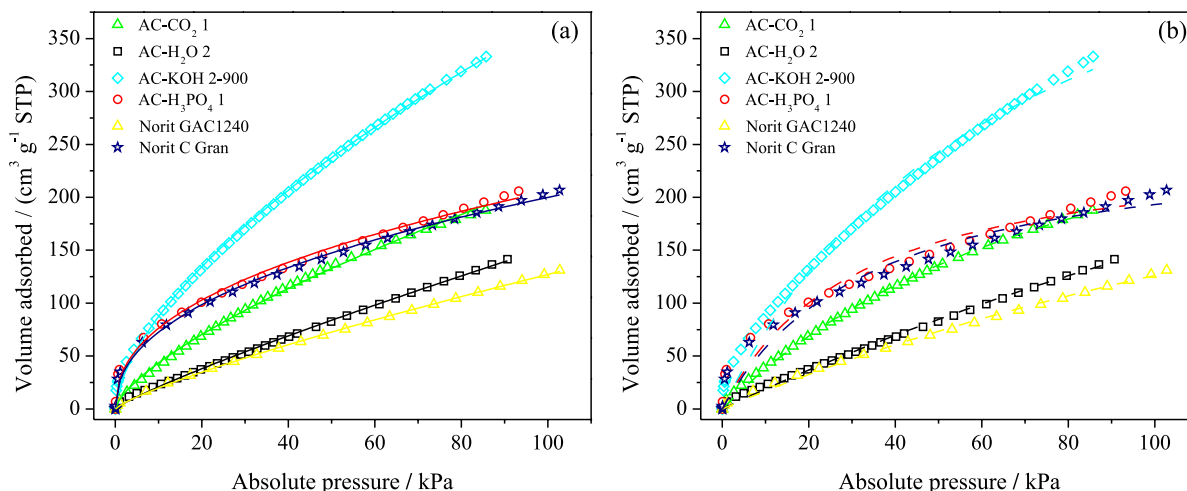


Figure 5. NH₃ adsorption isotherms at 20 °C for selected samples. Symbols: experimental data, solid line: Freundlich model (a), dash line: Langmuir model (b).

Table 7. NH₃ adsorption capacity of some adsorbents

Adsorbent	S_{BET} / (m ² g ⁻¹)	NH ₃ adsorption capacity / (mg g ⁻¹)
Activated carbon Merck ¹⁰¹	450	86
13X zeolite WE894 ¹⁰¹	365	158
Ordered mesoporous carbon ⁵⁹	798	109
Amberlyst 15 ¹⁰¹	225	193
Mesoporous alumina ¹⁰²	334	84
Silica nanoparticles ¹⁰²	366	18
CuCl ₂ BTA ¹⁰³	–	336
BC-400 ¹⁰⁰	3	190
AAC ¹⁰⁴	1267	121
AC-CO ₂ 1 ^a	1011	142
AC-H ₂ O 2 ^a	1511	107
AC-KOH 2-900 ^a	1823	252
AC-H ₃ PO ₄ 1 ^a	1986	156
Norit C Gran ^b	1328	157
Norit GAC 1240 ^b	1017	99

^aActivated carbon prepared in this work; ^bcommercial activated carbon. S_{BET} : BET surface area.

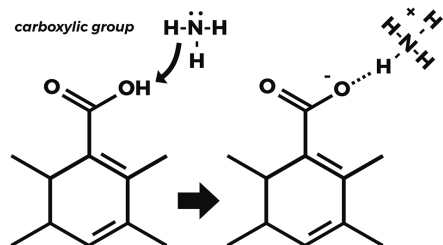


Figure 6. Interaction of ammonia with the carboxylic groups of AC.

on the surface of modified carbons favors NH₃ adsorption capacity and is related to the acid site type present. Due to the electronegative nature of nitrogen, the hydrogen atoms of the NH₃ molecule interact with the oxygen atoms linked

as hydroxyl (H–O) and carbonyl (C–O) groups on the surface because of the electrostatic forces (see Figure 6).¹⁰⁵

In this sense, TPD results of the AC-KOH 2-900 sample indicated the presence of a higher proportion of more acidic and less stable surface groups than other samples and explained the high NH₃ adsorption capacity obtained.⁹⁰ This assertion is established by correlating the adsorption capacity of NH₃ with the amount of more acidic surface groups (CO₂) that was released during the TPD test (Figure 7a). A linear trend was observed ($R^2 = 0.857$), although the increase in the NH₃ adsorption capacity with the more acidic surface oxygen groups was clearer for the AC-KOH 2-900 sample. In this sense, Gonçalves *et al.*⁸⁷ showed a linear correlation between the quantity of the more acidic oxygen surface groups and the NH₃ adsorption capacity in a commercial carbon (MAST).

In order to evaluate the influence of microporosity on the adsorption capacity of NH₃, these two parameters were plotted and are shown in Figure 7b. There is no relationship between the parameters that can be corroborated with the behavior of AC-KOH 2-900 and AC-H₃PO₄ 1 samples with an equal volume of micropores (ca. 0.73 cm³ g⁻¹) but very different NH₃ adsorption (252 vs. 156 mg g⁻¹, respectively). This tendency is identical if it is plotted the NH₃ adsorption against the surface area and mesopore volume. This behavior was also reported by Yeom *et al.*¹⁰² in a commercial AC, who indicated that the NH₃ adsorption capacity was unaffected by the surface area. However, other authors have established the preference for adsorbents with large surface areas and small pore sizes for NH₃ removal.^{101,106} Additionally, mesoporous samples have been proposed to adsorb ammonia because ordered and regular porous structures with well-defined channels favor the adsorption of NH₃.^{59,102} These different results suggest that the nature and preparation conditions

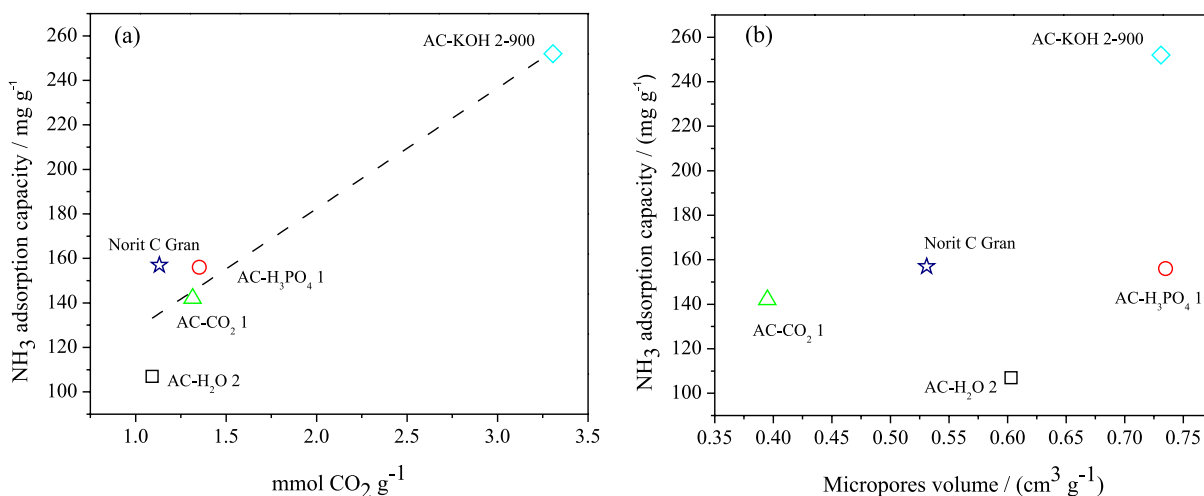


Figure 7. Relationship between NH_3 adsorption capacity, more acidic surface groups (a), and micropores volume (b).

Table 8. Fit of the experimental data of NH_3 adsorption at 20 °C to the Langmuir and Freundlich isotherms

Sample	Langmuir				Freundlich			
	$a_m / (\text{cm}^3 \text{ g}^{-1})$	$b / (\text{kPa}^{-1})$	ARE / %	R^2	$K_F / (\text{cm}^3 \text{ g}^{-1} \text{ kPa}^{-1/n})$	n	ARE / %	R^2
AC- CO_2 1	385.17	0.0109	18.85	0.9986	8.847	1.444	5.81	0.9989
AC- H_2O 2	667.92	0.0029	23.74	0.9965	2.871	1.159	20.08	0.9982
AC-KOH 2-900	579.21	0.0145	13.61	0.9903	20.918	1.610	6.52	0.9987
AC- H_3PO_4 1	256.18	0.0321	13.62	0.9714	28.333	2.324	5.52	0.9964
Norit C Gran	261.01	0.0285	15.78	0.9775	26.378	2.273	0.87	0.9981
Norit GAC 1240	448.69	0.0039	24.06	0.9979	3.097	1.239	13.03	0.9996

a_m : solid's maximum adsorption capacity; b : Langmuir adsorption constant related to the adsorption energy; ARE: average relative error; R^2 : coefficient of determination; K_F : constant relate to the relative capacity adsorption of adsorbent; n : constant of adsorption intensity.

of the sample influence the NH_3 adsorption. It could be improved by the surface area, porosity, and/or surface chemistry. Thus, from our results, the good adsorption behavior obtained for the KOH-activated sample could be explained by the combination of the high microporosity and adequate surface acidity. The activation with KOH effectively promoted the creation of oxygenated surface groups (carboxylic groups) and high microporosity (98%) with the best adsorption properties to remove NH_3 . The results obtained in this study indicated the best NH_3 adsorption for carbons chemically activated following the order: AC-KOH 2-900 > AC- H_3PO_4 1 > AC- CO_2 1 > AC- H_2O 2.

Regarding the adsorption models, the experimental data were adjusted to the Langmuir and Freundlich adsorption isotherm models. The Langmuir model implies monolayer adsorption on a homogeneous surface, with all active sites having the same energy and being equivalent. In addition, the Langmuir model considers dynamic equilibrium and no adsorbate interaction.¹⁰⁷ The Freundlich model is based on the following assumptions: (i) multilayer adsorption on heterogeneous surfaces, (ii) adsorbate interactions

and (iii) increase in the adsorption capacity with the concentration of the analyte.¹⁴

According to the results in Table 8, the lower ARE and the closest R^2 values to 1 indicate a good correlation for the Freundlich adsorption isotherm related to multilayer adsorption on a heterogeneous surface.¹⁴ Thus, the Freundlich model best describes NH_3 adsorption on prepared and reference ACs. In this sense, several authors have reported the same behavior in the fitting of the experimental data to the Freundlich model,^{59,108,109} and the value of $n > 1$ indicates favorable adsorption conditions.⁶⁷

Conclusions

In this study, ACs using olive stones were prepared. Depending on the activation method, the surface area of carbons ranges between 1000-1986 $\text{m}^2 \text{ g}^{-1}$, indicating that olive stone was successfully activated. Type I isotherms were observed in all the samples, characteristics of microporous solids; however, the isotherms obtained for steam and H_3PO_4 activated samples indicated the contribution of mesopores. KOH-AC reported the highest

iodine adsorptive capacity (1030 mg g^{-1}), which correlates with the high percentage of microporous obtained (98%). Surface area results showed the importance of the initial contact surface with the activating agent depending on whether the activation is in one or two steps, affecting the diffusion and removal of gaseous products from the sample. The presence of acidic functional groups (carboxylic, lactonic, phenolic) was observed by Boehm titration, FTIR, and TPD characterizations. It can explain the NH_3 adsorption capacity obtained, especially for AC-KOH 2-900 sample ($252 \text{ mg NH}_3 \text{ g carbon}^{-1}$). The TPD profile of KOH-AC showed the highest CO_2 evolution because more acidic surface groups were reported (carboxylic groups), and a linear trend was observed between the amount of NH_3 adsorbed and these surface groups. However, the surface area and micropore volume of samples did not affect the adsorption capacity of NH_3 . The NH_3 adsorption amounts of the physical and chemical prepared ACs are in the following order: AC-KOH 2-900 > AC- H_3PO_4 1 > AC- CO_2 1 > AC- H_2O 2. The good performance for the NH_3 adsorption obtained for the KOH-activated sample could be explained by the combination of the high microporosity and adequate surface acidity. The Freundlich model best fit the experimental data, implying that the multilayer adsorption on a heterogeneous surface was dominant.

Supplementary Information

Supplementary information (commercial ACs, Figure S1) is available free of charge at <http://jbcbs.sbq.org.br> as PDF file.

Acknowledgments

This work was supported by the Fundación para la Innovación Agraria FIA-Project PYT-2019-0158. N.E. acknowledges Fondecip No. EQM160070 and the Millennium Science Initiative Program NCN17_040. V.F. acknowledges ANID BASAL (grant number ACE210012 and FB 210015).

References

- Saleem, J.; Shahid, U. B.; Hijab, M.; Mackey, H.; McKay, G.; *Biomass Convers. Biorefin.* **2019**, *9*, 775. [Crossref]
- Demiral, H.; Demiral, I.; Karabacakoglu, B.; Tümsük, F.; *Chem. Eng. Res. Des.* **2011**, *89*, 206. [Crossref]
- Chang, C.-F.; Chang, C.-Y.; Tsai, W.-T.; *J. Colloid Interface Sci.* **2000**, *232*, 45. [Crossref]
- Rodríguez-Reinoso, F.; Molina-Sabio, M.; *Carbon N. Y.* **1992**, *30*, 1111. [Crossref]
- Yang, K.; Peng, J.; Xia, H.; Zhang, L.; Srinivasakannan, C.; Guo, S.; *J. Taiwan Inst. Chem. Eng.* **2010**, *41*, 367. [Crossref]
- Demiral, H.; Demiral, I.; Fatma, T.; Karabacako, B.; *Surf. Interface Anal.* **2008**, *40*, 616. [Crossref]
- Ubago-Pérez, R.; Carrasco-Marín, F.; Fairén-Jiménez, D.; Moreno-Castilla, C.; *Microporous Mesoporous Mater.* **2006**, *92*, 64. [Crossref]
- Román, S.; González, J. F.; González-García, C. M.; Zamora, F.; *Fuel Process. Technol.* **2008**, *89*, 715. [Crossref]
- González, J. F.; Román, S.; Encinar, J. M.; Martínez, G.; *J. Anal. Appl. Pyrolysis* **2009**, *85*, 134. [Crossref]
- Ahmedna, M.; Marshall, W. E.; Rao, R. M.; *Bioresour. Technol.* **2000**, *71*, 113. [Crossref]
- Lua, A. C.; Yang, T.; Guo, J.; *J. Anal. Appl. Pyrolysis* **2004**, *72*, 279. [Crossref]
- Bouchelta, C.; Medjram, M. S.; Bertrand, O.; Bellat, J.-P.; *J. Anal. Appl. Pyrolysis* **2008**, *82*, 70. [Crossref]
- Alau, K. K.; Gimba, C. E.; Kagbu, J. A.; *Arch. Appl. Sci. Res.* **2010**, *2*, 456. [Crossref]
- Luo, L.; Wu, X.; Li, Z.; Zhou, Y.; Chen, T.; Fan, M.; Zhao, W.; *R. Soc. Open Sci.* **2019**, *6*, 190523. [Crossref]
- Nagalakshmi, T. V.; Emmanuel, K. A.; Suresh Babu, C.; Chakrapani, C.; Divakar, P. P.; *Int. Lett. Chem., Phys. Astron.* **2015**, *54*, 189. [Crossref]
- Olivares-Marín, M.; Fernández-González, C.; Macías-García, A.; Gómez-Serrano, V.; *Appl. Surf. Sci.* **2006**, *252*, 5980. [Crossref]
- Laksaci, H.; Khelifi, A.; Trari, M.; Addoun, A.; *J. Cleaner Prod.* **2017**, *147*, 254. [Crossref]
- Hanum, F.; Bani, O.; Izdihar, A. M.; *IOP Conf. Ser.: Mater. Sci. Eng.* **2017**, *180*, 012149. [Crossref]
- Álvarez-Torrellas, S.; Peres, J. A.; Gil-Álvarez, V.; Ovejero, G.; García, J.; *Chem. Eng. J.* **2017**, *320*, 319. [Crossref]
- To, M.-H.; Hadi, P.; Hui, C. W.; Lin, C. S. K.; McKay, G.; *J. Mol. Liq.* **2017**, *241*, 386. [Crossref]
- Berrios, M.; Martín, M.; Martín, A.; *J. Ind. Eng. Chem.* **2012**, *18*, 780. [Crossref]
- Yakout, S. M.; Sharaf El-Deen, G.; *Arabian J. Chem.* **2016**, *9*, S1155. [Crossref]
- Yahya, M. A.; Al-Qodah, Z.; Nghah, C. W. Z.; *Renewable Sustainable Energy Rev.* **2015**, *46*, 218. [Crossref]
- Chile Oliva; *Informe Anual Mercado Nacional de Aceite de Oliva*; 2019. [Link] accessed in August 2022
- Foods from Chile; *La Industria del Aceite de Oliva en Chile. Informe de Sustentabilidad Chile Oliva*; Chile, 2019. [Link] accessed in August 2022
- Fundación para la Innovación Agraria; *Con Residuos del Aceite de Oliva Desarrollan Biocombustibles Sólidos y Carbones Descontaminantes*; Chile, 2020. [Link] accessed in August 2022
- Zabaniotou, A.; Stavropoulos, G.; Skoulou, V.; *Bioresour. Technol.* **2008**, *99*, 320. [Crossref]

28. Azbar, N.; Bayram, A.; Filibeli, A.; Muezzinoglu, A.; Sengul, F.; Ozer, A.; *Crit. Rev. Environ. Sci. Technol.* **2004**, *34*, 209. [Crossref]
29. Martínez, M. L.; Torres, M. M.; Guzmán, C. A.; Maestri, D. M.; *Ind. Crops Prod.* **2006**, *23*, 23. [Crossref]
30. Ioannidou, O.; Zabaniotou, A.; *Renewable Sustainable Energy Rev.* **2007**, *11*, 1966. [Crossref]
31. Wong, S.; Ngadi, N.; Inuwa, I. M.; Hassan, O.; *J. Cleaner Prod.* **2018**, *175*, 361. [Crossref]
32. González, M. T.; Rodríguez-Reinoso, F.; García, A. N.; Marcilla, A.; *Carbon N. Y.* **1997**, *35*, 159. [Crossref]
33. Enaime, G.; Ennaciri, K.; Ounas, A.; Baçaoui, A.; Seffen, M.; Selmi, T.; Yaacoubi, A.; *J. Mater. Environ. Sci.* **2017**, *8*, 4125. [Crossref]
34. Moreno-Castilla, C.; Carrasco-Marín, F.; López-Ramón, M. V.; Alvarez-Merino, M. A.; *Carbon N. Y.* **2001**, *39*, 1415. [Crossref]
35. Rodríguez-Reinoso, F.; Molina-Sabio, M.; González, M. T.; *Carbon N. Y.* **1995**, *33*, 15. [Crossref]
36. Baçaoui, A.; Yaacoubi, A.; Dahbi, A.; Bennouna, C.; Phan Tan Luu, R.; Maldonado-Hodar, F. J.; Rivera-Utrilla, J.; Moreno-Castilla, C.; *Carbon N. Y.* **2001**, *39*, 425. [Crossref]
37. Linares-Solano, A.; Rodríguez-Reinoso, F.; Molina-Sabio, M.; Lopez-Gonzalez, J. D.; *Adsorpt. Sci. Technol.* **1984**, *1*, 223. [Crossref]
38. Elmouwahidi, A.; Bailón-García, E.; Pérez-Cadenas, A. F.; Maldonado-Hódar, F. J.; Carrasco-Marín, F.; *Electrochim. Acta* **2017**, *229*, 219. [Crossref]
39. Molina-Sabio, M.; Rodríguez-Reinoso, F.; *Colloids Surf., A* **2004**, *241*, 15. [Crossref]
40. Mochizuki, T.; Kubota, M.; Matsuda, H.; D'Elia Camacho, L. F.; *Fuel Process. Technol.* **2016**, *144*, 164. [Crossref]
41. Petit, C.; Karwacki, C.; Peterson, G.; Bandosz, T. J.; *J. Phys. Chem. C* **2007**, *111*, 12705. [Crossref]
42. Busca, G.; Pistorino, C.; *J. Loss Prev. Process Ind.* **2003**, *16*, 157. [Crossref]
43. Guo, J.; Xu, W. S.; Chen, Y. L.; Lua, A. C.; *J. Colloid Interface Sci.* **2005**, *281*, 285. [Crossref]
44. Haimour, N. M.; Emeish, S.; *Waste Manage.* **2006**, *26*, 651. [Crossref]
45. Solum, M. S.; Pugmire, R. J.; Jagtoyen, M.; Derbyshire, F.; *Carbon N. Y.* **1995**, *33*, 1247. [Crossref]
46. Jagtoyen, M.; Derbyshire, F.; *Carbon N. Y.* **1998**, *36*, 1085. [Crossref]
47. Yang, T.; Lua, A. C.; *J. Colloid Interface Sci.* **2003**, *267*, 408. [Crossref]
48. Zhang, T.; Walawender, W. P.; Fan, L. T.; Fan, M.; Daugaard, D.; Brown, R. C.; *Chem. Eng. J.* **2004**, *105*, 53. [Crossref]
49. Lillo-Ródenas, M. A.; Cazorla-Amorós, D.; Linares-Solano, A.; *Carbon N. Y.* **2003**, *41*, 267. [Crossref]
50. Marsh, H.; Yan, D. S.; O'Grady, T. M.; Wennerberg, A.; *Carbon N. Y.* **1984**, *22*, 603. [Crossref]
51. ASTM D1506: *Standard Test Methods or Carbon Black - Ash Content*, West Conshohocken, 2020.
52. ISO 562: *Hard Coal and Coke-Determination of Volatile Matter*, Switzerland, 2010.
53. Leofanti, G.; Padovan, M.; Tozzola, G.; Venturelli, B.; *Catal. Today* **1998**, *41*, 207. [Crossref]
54. Blanco, E.; Sepulveda, C.; Cruces, K.; García-Fierro, J. L.; Ghampson, I. T.; Escalona, N.; *Catal. Today* **2020**, *356*, 376. [Crossref]
55. Gil, A.; Grange, P.; *Colloids Surf., A* **1996**, *113*, 39. [Crossref]
56. ASTM-D4607-14: *Standard Test Method for Determination of Iodine Number of Activated Carbon*, West Conshohocken, 2014.
57. Boehm, H. P.; *Carbon N. Y.* **1994**, *32*, 759. [Crossref]
58. Benzekri, M. B.; Benderdouche, N.; Bestani, B.; Douara, N.; Duclaux, L.; *J. Mater. Environ. Sci.* **2018**, *9*, 272. [Crossref]
59. Saha, D.; Deng, S.; *J. Colloid Interface Sci.* **2010**, *345*, 402. [Crossref]
60. Djelloul, C.; Hamdaoui, O.; *Desalin. Water Treat.* **2015**, *56*, 2966. [Crossref]
61. Hashem, A.; Al-Kheraije, K. A.; *J. Environ. Prot.* **2013**, *4*, 280. [Crossref]
62. Mediavilla, I.; Barro, R.; Borjabad, E.; Peña, D.; Fernández, M. J.; *Renewable Energy* **2020**, *160*, 374. [Crossref]
63. Bartocci, P.; D'Amico, M.; Moriconi, N.; Bidini, G.; Fantozzi, F.; *Energy Procedia* **2015**, *82*, 374. [Crossref]
64. Moubarik, A.; Grimi, N.; *Food Res. Int.* **2015**, *73*, 169. [Crossref]
65. Bedoui, A.; Souissi-Najar, S.; Ouederni, A.; *Int. J. Innovation Appl. Stud.* **2016**, *18*, 938. [Crossref]
66. Minkova, V.; Razvigorova, M.; Bjornbom, E.; Zanzi, R.; Budinova, T.; Petrov, N.; *Fuel Process. Technol.* **2001**, *70*, 53. [Crossref]
67. Gebreegziabher, T. B.; Wang, S.; Nam, H.; *J. Environ. Chem. Eng.* **2019**, *7*, 103234. [Crossref]
68. Hu, Z.; Srinivasan, M. P.; *Microporous Mesoporous Mater.* **2001**, *43*, 267. [Crossref]
69. Molina-Sabio, M.; González, M. T.; Rodríguez-Reinoso, F.; Sepúlveda-Escribano, A.; *Carbon N. Y.* **1996**, *34*, 505. [Crossref]
70. El-Hendawi, A.; *Appl. Surf. Sci.* **2009**, *255*, 3723. [Crossref]
71. Salame, I. I.; Bandosz, T. J.; *Ind. Eng. Chem. Res.* **2000**, *39*, 301. [Crossref]
72. Savova, D.; Apak, E.; Ekinci, E.; Yardim, F.; Petrov, N.; Budinova, T.; Razvigorova, M.; Minkova, V.; *Biomass Bioenergy* **2001**, *21*, 133. [Crossref]
73. Sun, K.; Jiang, J. C.; *Biomass Bioenergy* **2010**, *34*, 539. [Crossref]
74. Budinova, T.; Ekinci, E.; Yardim, F.; Grimm, A.; Björnbo, E.; Minkova, V.; Goranova, M.; *Fuel Process. Technol.* **2006**, *87*, 899. [Crossref]

75. László, K.; *Microporous Mesoporous Mater.* **2005**, *80*, 205. [Crossref]
76. Radovic, L.; *Surface Chemistry of Activated Carbon Materials: State of the Art and Implications for Adsorption, Surfaces of Nanoparticles and Porous Materials*; Schwarz, J.; Contescu, C., eds.; Marcel Dekker INC.: New York, 1999.
77. Guo, J.; Lua, A. C.; *Mater. Lett.* **2002**, *55*, 334. [Crossref]
78. Termoul, M.; Bestani, B.; Benderdouche, N.; Belhakem, M.; *Adsorpt. Sci. Technol.* **2006**, *24*, 375. [Crossref]
79. Esteves, B. M.; Morales-Torres, S.; Maldonado-Hódar, F. J.; Madeira, L. M.; *Chem. Eng. J.* **2021**, *411*, 128451. [Crossref]
80. Youssef, A.; El-Nabarawy, T.; El-Shafey, E.; *Carbon Lett.* **2006**, *7*, 1. [Crossref]
81. Şirazi, M.; Aslan, S.; *Chem. Eng. Commun.* **2021**, *208*, 1479. [Crossref]
82. Choi, S.; Choi, W.; Kim, S.; Lee, S.-Y.; Noh, I.; Kim, C. W.; *Biomater. Res.* **2014**, *18*, 6. [Crossref]
83. Dastgheib, S. A.; Rockstraw, D. A.; *Carbon N. Y.* **2001**, *39*, 1849. [Crossref]
84. Toles, C. A.; Marshall, W. E.; Johns, M. M.; *Carbon N. Y.* **1999**, *37*, 1207. [Crossref]
85. Mahmood, T.; Ali, R.; Naeem, A.; Hamayun, M.; Aslam, M.; *Process Saf. Environ. Prot.* **2017**, *109*, 548. [Crossref]
86. Benaddi, H.; Bandoş, T. J.; Jagiello, J.; Schwarz, J. A.; Rouzaud, J. N.; *Carbon N. Y.* **2000**, *38*, 669. [Crossref]
87. Gonçalves, M.; Sánchez-García, L.; de Oliveira Jardim, E.; Silvestre-Albero, J.; Rodríguez-Reinoso, F.; *Environ. Sci. Technol.* **2011**, *45*, 10605. [Crossref]
88. Figueiredo, J. L.; Pereira, M. F. R.; Freitas, M. M. A.; Órfão, J. J. M.; *Carbon N. Y.* **1999**, *37*, 1379. [Crossref]
89. Figueiredo, J. L.; Pereira, M. F. R.; *Catal. Today* **2010**, *150*, 2. [Crossref]
90. Ro, K. S.; Lima, I. M.; Reddy, G. B.; Jackson, M. A.; Gao, B.; *Agriculture* **2015**, *5*, 991. [Crossref]
91. Zhou, J. H.; Sui, Z.-J.; Zhu, J.; Li, P.; Chen, D.; Dai, Y.-C.; Yuan, W.-K.; *Carbon N. Y.* **2007**, *45*, 785. [Crossref]
92. Domingo-García, M.; Groszek, A. J.; López-Garzón, F. J.; Pérez-Mendoza, M.; *Appl. Catal., A* **2002**, *233*, 141. [Crossref]
93. Wu, X.; Radovic, L. R.; *Carbon N. Y.* **2006**, *44*, 141. [Crossref]
94. Song, J.; Zou, W.; Bian, Y.; Su, F.; Han, R.; *Desalination* **2011**, *265*, 119. [Crossref]
95. Cuhadaroglu, D.; Uygun, O. A.; *Afr. J. Biotechnol.* **2008**, *7*, 3706. [Crossref]
96. Han, R.; Zhang, L.; Song, C.; Zhang, M.; Zhu, H.; Zhang, L. J.; *Carbohydr. Polym.* **2010**, *79*, 1140. [Crossref]
97. Fanning, P. E.; Vannice, M. A.; *Carbon N. Y.* **1993**, *31*, 721. [Crossref]
98. Guo, J.; Lua, A. C.; *Microporous Mesoporous Mater.* **1999**, *32*, 111. [Crossref]
99. Pérez Marín, A. B.; Aguilar, M. I.; Meseguer, V. F.; Ortuño, J. F.; Sáez, J.; Lloréns, M.; *Chem. Eng. J.* **2009**, *155*, 199. [Crossref]
100. Asada, T.; Ohkubo, T.; Kawata, K.; Oikawa, K.; *J. Heal. Sci.* **2006**, *52*, 585. [Crossref]
101. Helminen, J.; Helenius, J.; Paatero, E.; Turunen, I.; *J. Chem. Eng. Data* **2001**, *46*, 391. [Crossref]
102. Yeom, C.; Kim, Y.; *Environ. Eng. Res.* **2017**, *22*, 401. [Crossref]
103. Rieth, A. J.; Dinca, M.; *J. Am. Chem. Soc.* **2018**, *140*, 3461. [Crossref]
104. Park, S.-J.; Kim, K.-D.; *J. Colloid Interface Sci.* **1999**, *212*, 186. [Crossref]
105. Shan, X.-m.; Zhu, S.-q.; Zhang, W.-h.; *J. China Univ. Min. Technol.* **2008**, *18*, 261. [Crossref]
106. Saha, D.; Deng, S.; *J. Colloid Interface Sci.* **2010**, *348*, 615. [Crossref]
107. Sangon, S.; Hunt, A. J.; Attard, T. M.; Mengchang, P.; Ngernyen, Y.; Supanchaiyamat, N.; *J. Cleaner Prod.* **2018**, *172*, 1128. [Crossref]
108. Liang, P.; Yu, H.; Huang, J.; Zhang, Y.; Cao, H.; *MATEC Web Conf.* **2016**, *67*, article 07006. [Crossref]
109. Hayhurst, D. T.; *Chem. Eng. Commun.* **1980**, *4*, 729. [Crossref]

Submitted: March 27, 2022

Published online: August 10, 2022

